International Journal of Nanomedicine Dovepress

Open Access Full Text Article ORIGINAL RESEARCH

Black Phosphorus Nanosheets-Loaded Single-Atom Gold Nanoenzymes for Enhanced Photodynamic Therapy of Hepatocellular Carcinoma

Jianmeng Zhu[1], Hongqin Wang[1], Kaiqiang Li[2], Xiuze Yuan[3], Wenzhong Hong[1]

[1]Clinical Laboratory of Chun'an First People's Hospital, Zhejiang Provincial People's Hospital Chun'an Branch, Hangzhou, Zhejiang, People's Republic of China; [2]Laboratory Medicine Center, Allergy Center, Department of Transfusion Medicine, Zhejiang Provincial People's Hospital (Affiliated People's Hospital), Hangzhou Medical College, Hangzhou, Zhejiang, People's Republic of China; [3]Pharmacy Department of Chun'an First People's Hospital, Zhejiang Provincial People's Hospital Chun'an Branch, Hangzhou, Zhejiang, People's Republic of China

Correspondence: Kaiqiang Li, Laboratory Medicine Center, Allergy Center, Department of Transfusion Medicine, Zhejiang Provincial People's Hospital (Affiliated People's Hospital), Hangzhou Medical College, 158 Shangtang Road, Hangzhou, Zhejiang, 310014, People's Republic of China, Tel/Fax +86 571 8589 3270, Email likaiqiang@hmc.edu.cn

Background: Conventional treatments for hepatocellular carcinoma (HCC) lack efficacy and targeting abilities. Photodynamic therapy (PDT) has emerged as a promising alternative for targeted and minimally invasive tumor treatments. However, many biomaterials used in PDT pose biosafety concerns and insufficient enzyme activity often leads to limited reactive oxygen species (ROS) production, resulting in poor PDT efficacy. Single-atom nanoenzymes have attracted much research attention as a novel type of high-performance nanoenzymes.

Methods: In this study, we prepared black phosphorus nanosheets (BP) with good biocompatibility as a platform and loaded single-atom gold nanoenzymes onto BP nanosheets to treat HCC. To enhance the stability and targeting ability of the nanohybrid, it was PEGylated and modified with folate (FA) targeting molecules.

Results: The designed BP/single-atom nanoenzyme platform can target tumor tissues and generate substantial amounts of reactive oxygen species (ROS), demonstrating biocompatibility and improved catalytic activity.

Conclusion: The nanoplatform effectively targets HCC and enhances PDT efficacy by increasing ROS production, offering a promising approach for HCC treatment.

Keywords: tumor treatment, photodynamic therapy, hepatocellular carcinoma, black phosphorus, single-atom gold

Introduction

Hepatocellular carcinoma (HCC) is a common malignancy worldwide. Conventional radiotherapy and chemotherapy feature low efficacy, adverse side effects, and poor precision, making the treatment of HCC challenging.[1] Photodynamic Therapy (PDT), a novel tumor treatment method, uses photosensitizing agents and light activation to generate reactive oxygen species (ROS), inducing tumor cell damage and death. This approach provides specific tumor targeting, low invasiveness, low systemic toxicity, and repeatability.[2] However, many biomaterials used in PDT pose biosafety risks because of their slow biodegradation rates and accumulation of toxic materials. In addition, the insufficient enzymatic activity of the PDT system results in poor ROS toxicity and limited antitumor efficacy.[3,4] Therefore, developing biocomposites with favorable biocompatibility and elevated catalytic activity is crucial.

Black phosphorus (BP) is a two-dimensional nanomaterial that has gained significant attention because of its unique structure consisting of corrugated planes of P atoms. Optimizing the structure yields high-precision optical response qualities and anisotropic charge transport, making BP a suitable photosensitization candidate for photodynamic and photothermal therapy (PTT).[5,6] Furthermore, BP degrades very slowly in normal cells but rapidly in tumor cells under

Received: 28 September 2024
Accepted: 22 November 2024
Published: 26 November 2024

conditions of high oxidative stress and acidity.[7] Since phosphorus is an essential element in living organisms, the degradation products of BP are nontoxic to humans.[8,9] BP nanosheets can be easily functionalized with biocompatible molecules,[10] such as polyethylene glycol (PEG),[11] which improves their stability in tumor cells and reduces the risk of immune response.[12] Thus, it exhibits specific antitumor properties and biocompatibility.

However, single BP has poor peroxidase activity and limited ROS generation, constraining its PDT efficacy.[13] Natural peroxidases rapidly denature during storage and handling, and their BP binding is volatile.[14] Fortunately, as a favored nanomaterial, gold nanoenzymes are highly catalytic, biocompatible, and pH-dependent.[15] Gold nanoenzymes can effectively decompose hydrogen peroxide (H_2O_2) to generate hydroxyl radicals (•OH) under the acidic environment of the tumor. Meanwhile, BP can generate large amounts of singlet oxygen ($^1O_2$) under near-infrared (NIR) light irradiation. These two nanomaterials synergistically improve PDT efficacy.[16] Smaller gold nanoparticles (AuNPs) have more low-coordinated gold atoms, which enhance catalytic activity. They do not cause significant immune reactions or toxicity in living organisms.[17,18] Moreover, single-atom gold nanoenzymes technology allows AuNPs to work at the atomic level, and all individual gold atoms are highly efficient active sites due to the universal coordination environment.[19] Their tiny size makes biomedical functionalization and targeted delivery easy.[20,21] In addition, AuNPs are superior photothermal converters to other metal-based nanoenzymes and can be employed as PTT therapeutics.[22,23] The thermal effect further enhances PDT efficacy by increasing enzymatic activities and ROS production.[18,24]

Here, we aimed to construct PEGylated BP@Au@FA (folate) nanoplatforms (BP@Au@FA-PEG) for enhanced photodynamic therapy of HCC. As shown in Scheme 1, BP nanosheets were prepared using the stripping method[25] and loaded with single-atom Au nanoparticles (BP@Au). Then, FA-targeting molecules with PEG chains were modified on BP@Au, which enhanced the stability of the BP nanosheets without affecting their photosensitive properties. FA can recognize folate receptors on the surface of hepatocellular carcinoma cells to achieve specific targeting. The nanoplatform enters the cell through receptor-mediated endocytosis. Single-atom gold peroxidase breaks down H_2O_2 and generates a large amount of •OH in the acidic environment of tumor cells. Under 660 nm laser irradiation, BP produces $^1O_2$; Au and BP convert light to heat, improving photodynamic therapy and peroxidase activity. After treatment, owing to the high oxidative stress and acidic conditions inside the tumor cells, BP degrades to nontoxic phosphate, and gold atoms

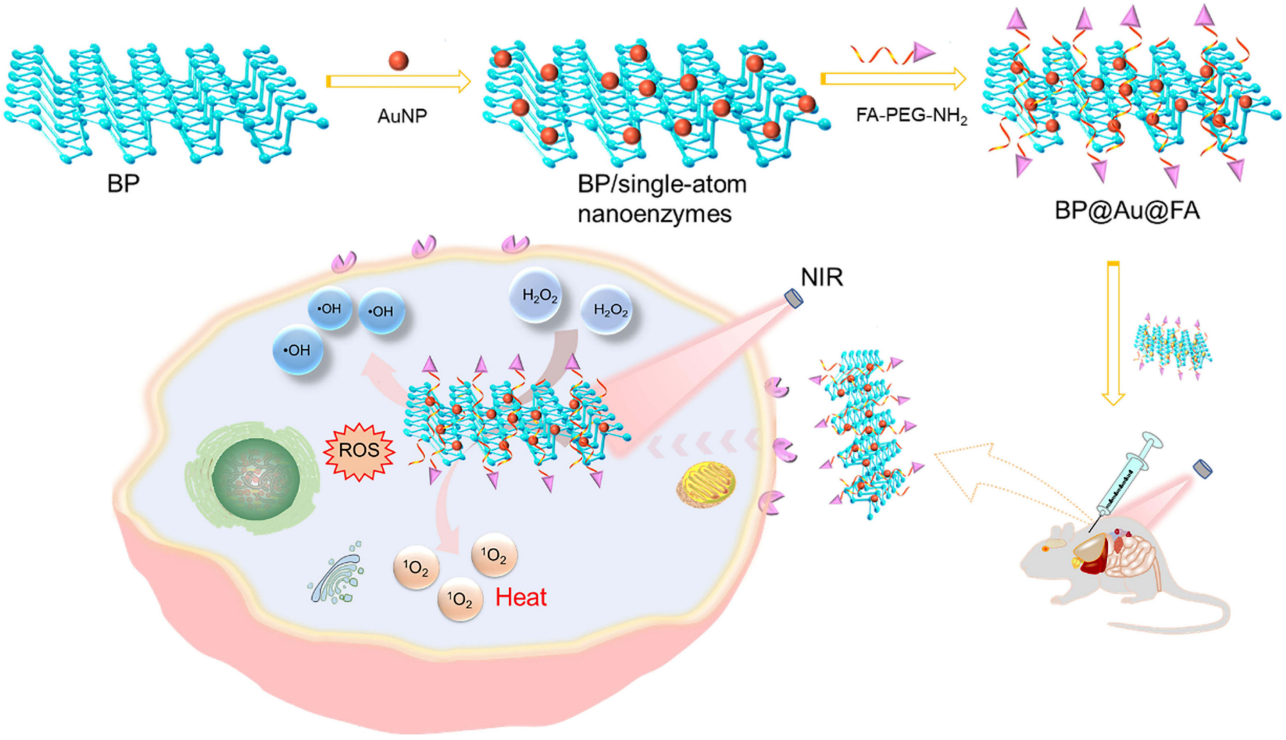

Scheme 1 Principles of the synthesis and tumor treatment of BP@Au@FA-PEG.

are eliminated without biological toxicity. BP@Au@FA-PEG nanohybrids exhibited superior photodynamic therapy efficiency and biocompatibility, offering great potential for clinical translation.

Materials and Methods

Materials

Bulk BP crystals were purchased from Nanjing Nanoeast Biotechnology Co. Ltd. 2′,7′-dichlorodihydrofluorescein diacetate (DCFH-DA), CCK-8 cytotoxicity assay kit, calcein-AM, propidium iodide (PI), and $HAuCl_4$ solution were purchased from Sigma-Aldrich; Merck KGaA. FA-PEG-NH_2, Cy5.5-FA-PEG-NH_2, and Cy5.5-PEG-NH_2 were purchased from Tanshui Technology Co. Ltd. (Guangzhou, China). All reagents and solvents were analytically pure and were used as received without further purification. Chinese Academy of Science Cell Bank (Shanghai, China) supplied Huh-7 cells. The cells were grown in Dulbecco's modified Eagle's medium (Gibco) supplemented with fetal bovine serum, penicillin, and streptomycin. Female BALB/c nude mice (6–8 weeks old) were obtained from Jiangsu Jitaike Biopharmaceuticals Co., Ltd. (Nanjing, China). The Laboratory Animal Management and Ethics Committee of Zhejiang Provincial People's Hospital approved this experimental protocol. Animal experiments were conducted in accordance with the guidelines provided by the Committee. These guidelines include those for animal welfare.

Preparation of Ultrathin BP

In an ice bath, 50 mg of bulk BP was mixed with 50 mL of water bubbled with argon and sonicated for 8 h. The brown suspension was then centrifuged at 150 × g for 10 min to remove any remaining unexfoliated particles. The supernatant was washed with hexane, chloroform, and ethanol after 10 min of centrifugation at 3000 rpm. After three washes, the BP nanosheets were vacuum-dried for further use.

Synthesis of BP@Au Nanosheets

For BP@Au nanosheet production, 200 mg of BP nanosheets were dispersed in 260 mL of ethanol with N2 protection. Subsequently, a two-channel syringe pump was used to introduce 15 mL $HAuCl_4$ (0.2 mm) into the BP nanosheet solution. The process was carried out at room temperature for 4 h under N2 shielding. The mixture was centrifuged, washed thrice with ethanol, and dried under a vacuum.

FA-PEG Modified BP@Au

A solution containing 2 mg BP@Au nanoparticles dispersed in 10 mL ultrapure water was combined with 10 mg FA-PEG-NH_2 (or Cy5.5-FA-PEG-NH_2, Cy5.5-PEG-NH_2). Following sonication for 10 min and stirring for 5 h, surplus molecules were eliminated by centrifugation (15000 rpm, 10 min). Therefore, BP@Au@FA-PEG, Cy5.5-BP@Au@FA-PEG, and Cy5.5-BP@Au-PEG were obtained.

Characterizations

The morphologies of the nanoparticles were characterized by transmission electron microscopy (TEM, JEM-2100F, JEOL, Japan). Raman spectra were obtained using an HR Labram microspectrometer (LabRAM HRevolution, France). Zetasizer Nano ZS680 (Malvern, UK) was used to measure the size and zeta potential of the nanomaterials. The absorbance values of Cy5.5 labeled nanoparticles were measured using a microplate reader (VersaMax; Molecular Devices). The thickness of the nanoparticles was analyzed by atomic force microscopy (AFM; Bruker, nanoIR3, German).

Assessment of ROS Generation Capacity of the Nanohybrids

The hydroxyl radical (•OH) and singlet oxygen ($^1O2$) generating capacities of BP@Au@FA-PEG were detected by electron spin resonance (ESR) spectroscopy (JES-X30, Japan). Singlet oxygen generation was analyzed using SOSG (Singlet Oxygen Sensor Green). SOSG (4 μM in PBS) containing 1% DMSO was mixed with five groups of samples (Group 1: ultrapure water under 660 NIR laser irradiation (1 W cm^{-2}, 10 min); Group 2:2 μM

BP@Au@FA-PEG; Group 3:2 μM BP@Au @FA-PEG under 660 laser irradiation; and Group 4:2 μM BP@Au@FA-PEG under 660 laser irradiation with 80 μM H_2O_2). The fluorescence spectra were measured using ESR spectroscopy (SOSG fluorescence, $\lambda_{ex}/\lambda_{em}$ = 488/525 nm). Each group contained three samples.

For •OH detection, BMPO (50 mm) was used as the capturing agent and mixed with three groups of samples (Group 1:80 μM H_2O_2 solution; Group 2:2 μM with 80 μM H_2O_2, Group 3:2 μM BP@Au@FA-PEG under 660 laser irradiation with 80 μM H_2O_2). The ESR spectra were measured under the following settings: 1 G field modulation, 20 mW microwave power, and a 200 G scan range. Each group contained three samples.

Intracellular ROS Assay

DCFH-DA was used as a fluorescent probe to capture ROS in the Huh7 cells. Huh7 cells were seeded in glass-bottom dishes at a density of 5×10^5 cells/well and incubated at 37 °C for 24h with 5% CO_2. Huh7 cells were co-incubated for 10 h with Group 1:500 μL of BP@Au@FA-PEG(2 μM), Group 2:660 nm NIR laser (1 W cm^{-2}, 10 min), Group 3: BP@Au@FA-PEG + NIR, Group 4: BP@Au@FA-PEG + H_2O_2 (80 μM), and Group 5: BP@Au@FA-PEG + NIR + H_2O_2. Next, the uninternalized nanoparticles were removed, and DCFH-DA (20 μM) was added and incubated for another 30 min. After washing, Huh7 cells were observed using fluorescence microscopy (excitation: 488 nm, emission: 515–545 nm).

Cytofluorescence Assay

Huh7 cells were seeded on 20 mm glass coverslips in six-well plates at a density of 5×10^5 cells per well. To investigate the cellular uptake of BP@Au@FA-PEG, the cells were incubated with Cy5.5-BP@Au@FA-PEG or Cy5.5-BP@Au@-PEG (2 μM) for 1 h. Cellular uptake was observed under a fluorescence microscope. The cells were then washed with PBS and stained with LysoGreen for 20 min and DAPI for 5 min. After washing with an anti-fluorescence quencher, cells were fixed with 4% paraformaldehyde and imaged using a fluorescence microscope.

In vitro Cytotoxicity Assays

The in vitro antitumor effect of BP@Au@FA-PEG was examined by calcein-AM/PI cell staining and cell viability assays. Huh7 cells (5×10^4 cells/well) were seeded in a glass-bottom petri dish, incubated in the culture medium for 12 h, and then co-incubated for 18 h with Group 1:500 μL of BP@Au@FA-PEG(2 μM); Group 2500 μL of H_2O_2 (80 μM); Group 3660 nm NIR laser (1 W cm^{-2}, 10 min); Group 4: BP@Au@FA-PEG + NIR; Group 5: BP@Au@FA-PEG + H_2O_2; and Group 6: BP@Au@FA-PEG + NIR + H_2O_2. Huh7 cells were washed several times with PBS and stained with calcein-AM and PI. After 15 min, the staining solution was removed, and the cells were washed with PBS and observed by fluorescence microscopy. A *NucleoCounter®NC-250*™ Automated Cell Counting System (ChemoMetec A/S, Allerod, Denmark) was used to determine the viability of each sample.

In vivo Antitumor Study

Huh7 cells (200 μL, 5×10^6) were injected into the axilla of the front legs of mice. When the tumors reached 100 mm^3, tumor-bearing mice were randomly divided into four groups (n = 6 mice per group). The formula for tumor volume is V = 1/2 L × W^2 (L is the length of the tumor and W is the width of the tumor). The mice were treated every 3 days in four ways: Group 1 received PBS injection, Group 2 was irradiated with 660 nm NIR laser (1 W cm−2, 10 min), Group 3 received 500 μL of BP@Au@FA-PEG (2 μM), and Group 4 received the same injection as Group 3 and NIR irradiation. The experiments were performed using intratumoral injections. Small silicon optical fibers (Thorlabs, Shanghai, China) were inserted near the liver via a percutaneous route for NIR irradiation. Tumor size and body weight were measured every other day. The mice were euthanized according to the animal welfare requirements on day 14. The major organs (including the heart, liver, spleen, lungs, and kidneys) and tumors were separated by H&E and DAPI staining. Tumor weights were measured. To test survival, the mice were treated again and not euthanized. Survival curves were plotted based on the survival times of the mice.

Statistical Analysis

Data are presented as the mean ± SD. The independent samples *t*-test determined statistical significance, with $p< 0.05$(*) indicating a statistically significant difference, and highly significant when $p< 0.01$ (**).

Results and Discussion

Characterization

BP nanosheets were prepared using liquid-exfoliated bulk BP. Transmission electron microscopy (TEM) revealed homogenous freestanding BP nanosheets with lateral sizes of several hundred nanometers (Figure 1a). BP@Au nanosheets were created by infusing $HAuCl_4$ solution into ethanol and BP nanosheets using a syringe pump under nitrogen protection. $HAuCl_4$ was reduced to Au nanoparticles, which spontaneously and uniformly covered BP nanosheets. Because phosphorus oxides and phosphoric acid strongly chelate Au, the oxidized BP nanosheets stabilize the Au nanoparticles. Figure 1b–d demonstrated that the gold atoms uniformly decorated the BP nanosheets.

Figure 1e displays three typical Raman peaks of BP corresponding to the A1 g (out-of-plane), B_{2g} (in-plane), and A2 g (in-plane) vibration modes at 358 cm^{-1}, 434, and 461 cm^{-1}, respectively. After Au modification, the Raman scattering peaks shift towards lower wavenumbers; this may be due to the reduction reaction that causes BP to undergo contraction and structural changes, such as a decrease in the lattice constant. Figure 1f shows the TEM image of FA-PEG-modified BP@Au. FA-PEG was uniformly loaded onto BP@Au and did not cause noticeable structural changes in BP@Au nanosheets. We further used Cy5.5 fluorescently labeled FA-PEG to verify the synthesis of hybrid nanomaterials. As shown in Figure 1g, BP@Au displays no fluorescence. The hybrid nanomaterials exhibited sheet-like uniform red fluorescence under a fluorescence microscope. The fluorescence intensity of the hybrid nanomaterials was measured using a SPARK 10 M fluorescence microplate reader (Tecan). The fluorescence values of BP@Au@FA-PEG-Cy5.5 (1029) and Au@BP (5) were compared (Figure 1h), confirming the successful loading of FA-PEG onto BP@Au. We further analyzed the thickness of the nanomaterials (Figure 2) and found that the average thickness of BP@Au (~3.0 nm) was close to that of BP (~2.5 nm), suggesting that the surface of BP was covered with gold atoms. The average thickness of BP@Au@FA-PEG was about 8.5 nm, and the increased thickness was attributed to the successful modification of PEG-FA molecules, which improved the stability and targeting of the nanoparticles.

ROS Productivity and Cellular Uptake

Figure 3a shows that NIR(660 nm, 1 W cm−2, 10 min) and BP@Au@FA-PEG alone did not generate $^1O_2$. Upon exposure to NIR and H_2O_2, BP@Au @FA-PEG exhibited the highest $^1O_2$. In this experiment, H_2O_2 was added to model the tumor

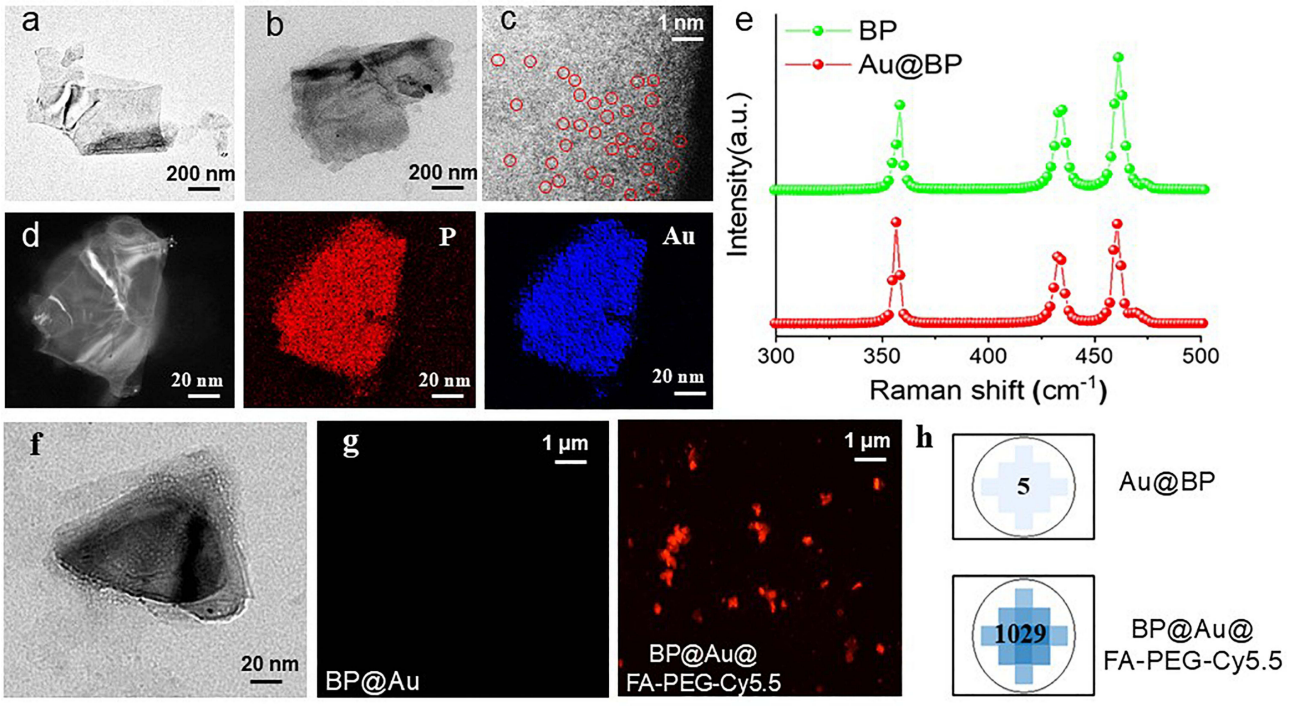

Figure 1 Characterization of nanomaterials. TEM images of BP nanosheets (**a**) and BP@Au (**b**); HAADF-STEM (High-angle annular dark-field scanning transmission electron microscopy) (**c**) image of BP@Au nanoparticles, and the elemental mapping of P and Au (**d**); Raman spectra of BP and BP@Au (**e**); TEM image of BP@Au@FA-PEG (**f**), Fluorescence microscopy images of BP@Au and BP@Au@FA-PEG-Cy5.5 (**g**), and Fluorescence intensity values for BP@Au and BP@Au@FA-PEG-Cy5.5 (**h**).

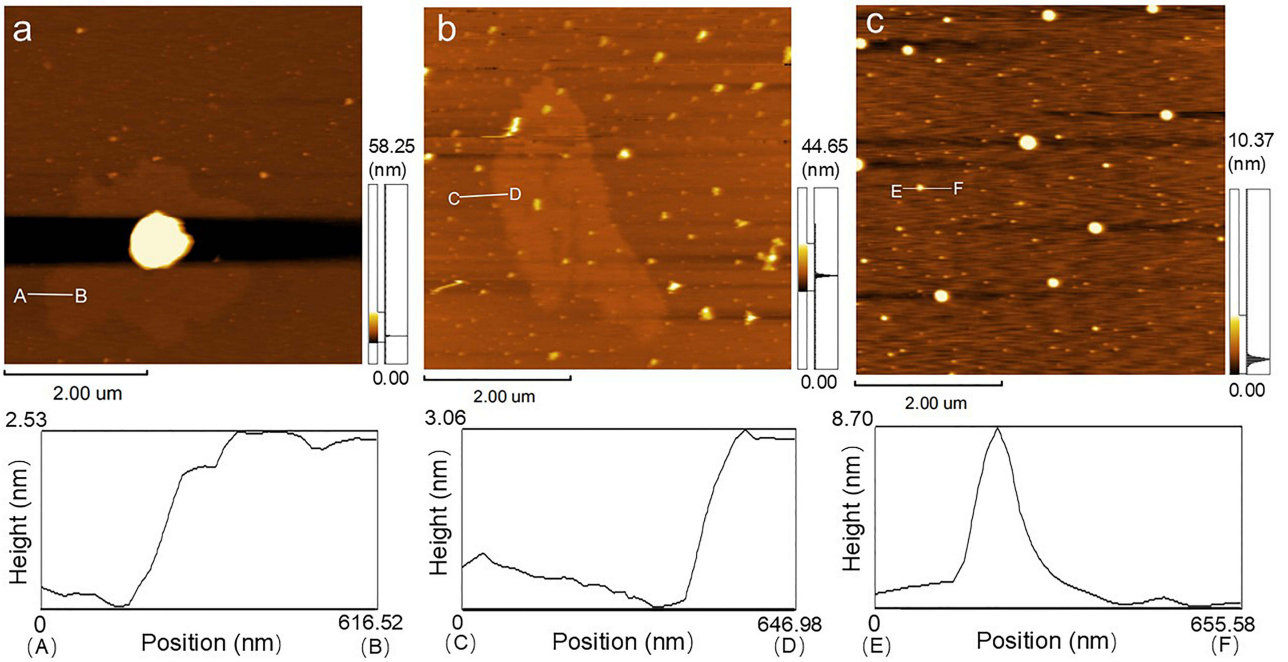

Figure 2 AFM analysis of nanomaterials. AFM images of BP (**a**), BP@Au (**b**), BP@Au@FA-PEG (**c**), and their corresponding height analysis along the white lines.

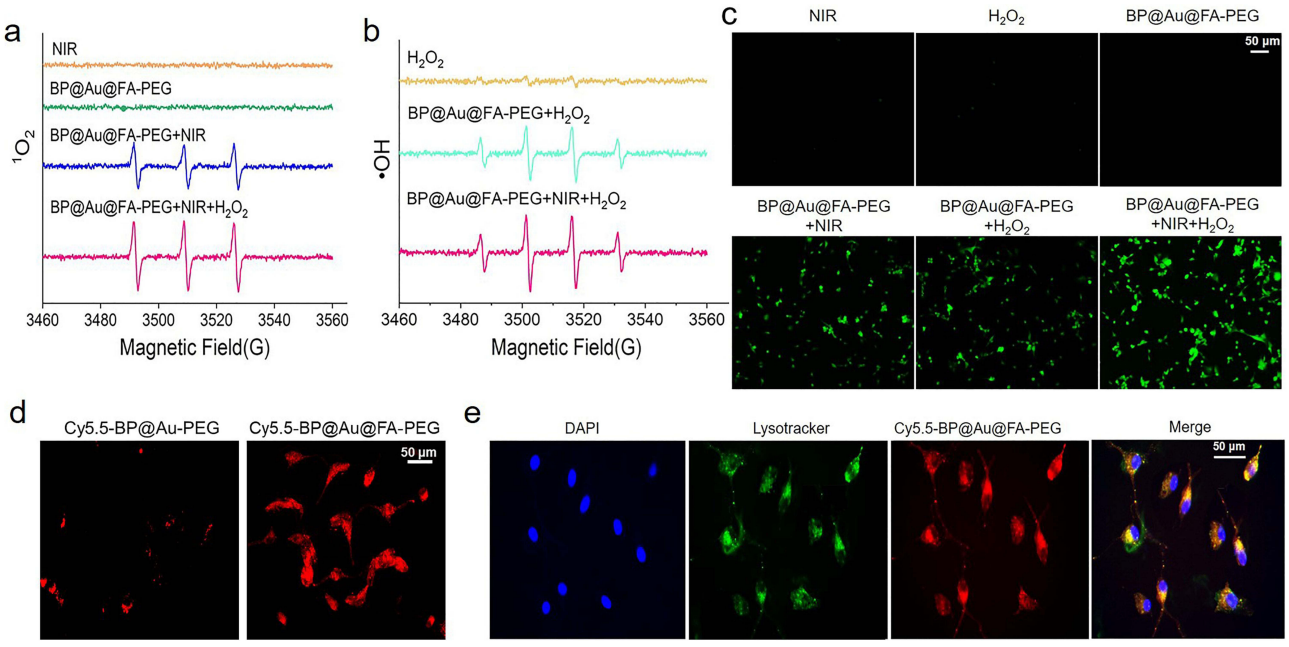

Figure 3 Cytofluorescence assay of nanomaterials. ESR spectrogram of $^1O_2$ (**a**) and •OH generation (**b**). DCFH-DA cell-staining for detection of intracellular ROS generation (**c**). Fluorescent images of Huh 7 cells treated with Cy5.5-BP@Au@FA-PEG and Cy5.5-BP@Au-PEG (**d**). Fluorescent images of cellular uptake of BP@Au@FA-PEG under different fluorescence channels (Red: Cy5.5 fluorescence; Blue: DAPI staining of nuclei; Green: LysoGreen staining of lysosome) (**e**).

microenvironment. H_2O_2 in tumor cells can interact with BP to facilitate the generation of $^1O_2$, thereby augmenting the effectiveness of photodynamic therapy. Figure 3b shows that the nanohybrid generated •OH in the presence of H_2O_2 and that NIR irradiation increased •OH production. Noble metal nanoparticles mimic intrinsic peroxidase and catalase activities by switching the pH. Free radicals, particularly •OH species, contribute to the peroxidase activity of Au nanoparticles. Collisions between the H_2O_2 molecules and Au surfaces break the O-O link, generating •OH. The pH of the surrounding media affects subsequent formation. Studies have shown that Au nanoparticles generate •OH through enhanced peroxidase activity at low

pH. Therefore, BP@Au@FA-PEG exhibits intense peroxidase activity in a tumor-acidic environment, leading to ROS generation. NIR enhanced the production of •OH, probably owing to the photothermal effect that enhanced the peroxidase activity of single-atom Au and the photodynamic reaction of BP nanosheets.

Fluorescence microscopy can be used to monitor fluorescent probe-labelled cells for intracellular ROS detection. DCFH-DA fluorescent probes can immediately react with ROS and produce a green fluorescent signal, allowing researchers to measure the intracellular ROS levels and distribution. Figure 3c shows that none of the three controls (NIR, H_2O_2, and BP@Au@FA-PEG) generated ROS, whereas BP@Au@FA-PEG+NIR+H_2O_2 displayed a higher green fluorescence intensity than BP@Au@FA-PEG+NIR or BP@Au@FA-PEG+H_2O_2, implying the highest level of ROS generation within the cells. To study the in vitro cellular targeting and uptake of nanoparticles. The nanoparticles with Cy5.5 fluorescent dye were observed after co-incubation with the cells. Figure 3d shows that FA-modified BP@Au enhanced cell targeting. Figure 3e shows that BP@Au@FA-PEG was effectively taken up by cells.

In vitro Antitumor Effects

Calcein-AM is a cell-permeable staining reagent that is susceptible to degradation by esterases, resulting in the formation of calcein and subsequent emission of green fluorescence. PI is a staining reagent for deceased cells that specifically binds to DNA within the nucleus and emits red fluorescence, thereby quantifying dead cells. Using these two dyes, we were able to detect cell survival visually and accurately. As shown in Figure 4a and b, the groups (BP@Au@FA-PEG, NIR laser, and H_2O_2) did not eliminate tumor cells. The BP@Au@FA-PEG + NIR group killed some cells owing to the production of $^1O2$ by BP, and •OH was difficult to produce because pH could not activate the peroxidase-like activity of single-atom gold. For the BP@Au@FA-PEG + H_2O_2, single-atom Au yielded a large amount of •OH owing to the

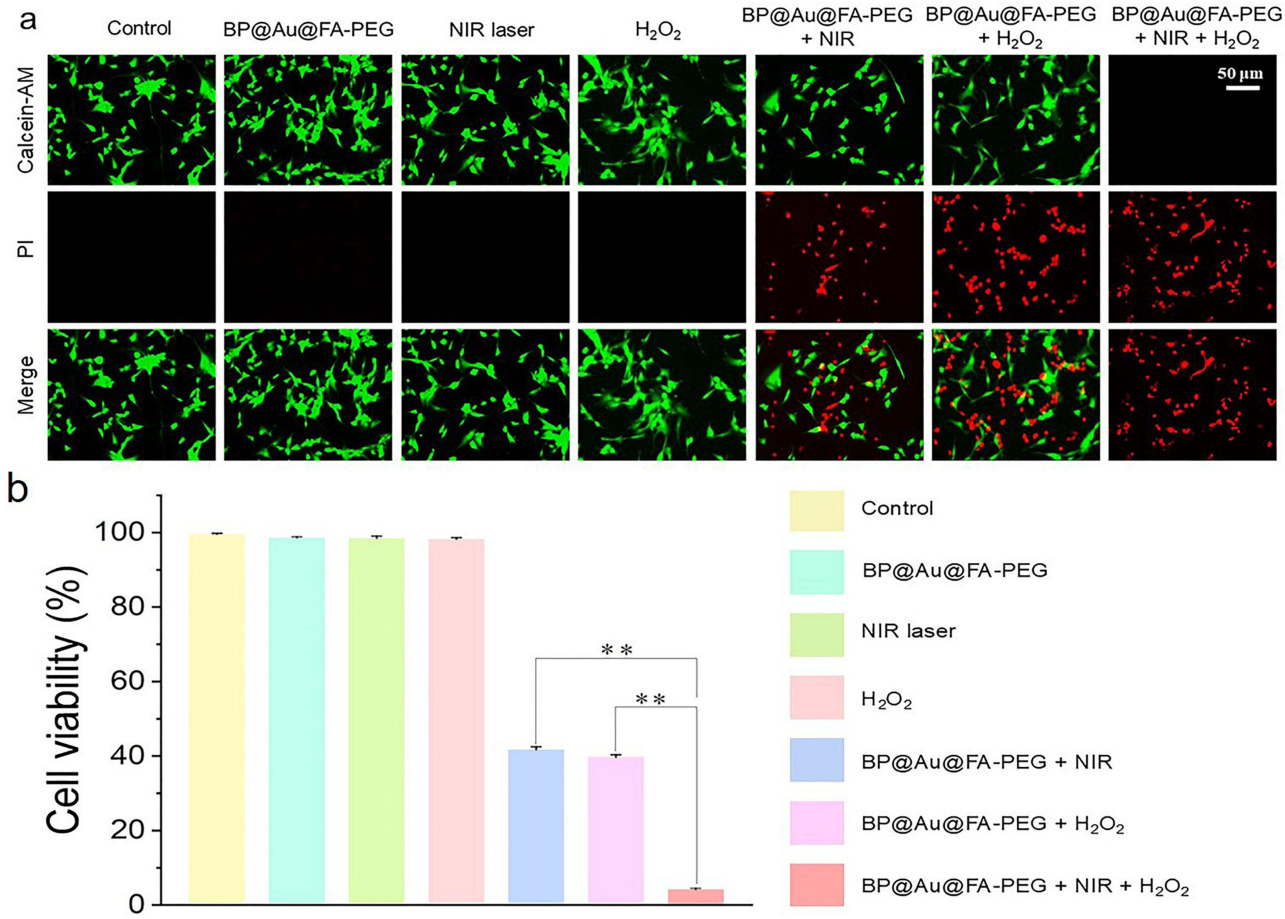

Figure 4 Evaluation of tumor cell killing by photodynamic therapy system in vitro. Fluorescent images of cell survival (**a**). Calcein-AM (living cells, green fluorescence), PI (dead cells, red fluorescence). Histogram of cell viabilities for each group (**b**). ** indicates a highly significant difference ($p< 0.01$).

decrease in pH, which caused more cell death. For group BP@Au@FA-PEG + NIR+ H_2O_2, the most potent photodynamic effect of BP@Au@FA-PEG was induced by the synergistic action of BP and monoatomic gold; therefore, the most cell deaths were observed.

In vivo Photodynamic Therapy of Hepatocellular Carcinoma

As shown in Figure 5a, group (3) exhibited the smallest tumor volume, owing to the enhanced photodynamic effect. The PBS group without any treatment had the largest tumor volume. NIR alone displayed little therapeutic effect on the tumor, and the tumor volume of group (3) was larger than that of group (4) because BP@Au@FA-PEG relied on the enzymatic reaction of single-atom gold to produce ROS for tumor elimination in the absence of NIR. Figure 5b shows the body weight of the mice. For groups (3) and (4), the weights of mice displayed negligible fluctuations during treatment, indicating that BP@Au@FA-PEG did not cause acute injury or noticeable side effects in mice. At the later stage of treatment, the weights of mice in the PBS and NIR groups exhibited a relatively apparent downward trend owing to the deterioration in the health of mice caused by the progression of tumors, leading to weight loss. Figure 5c and d present statistical data on tumor weight and corresponding images of tumor tissue in mice upon sacrifice. Enhanced photodynamic therapy can effectively eliminate tumors, and the weights were substantially lower than those of the other groups.

We further employed HE and DAPI staining of tumor tissues to evaluate the BP@Au@FA-PEG + NIR therapeutic system. As depicted in Figure 5e, group (4) exhibited the highest eradication of cancer cells, and the number of tumor cell nuclei was significantly reduced compared to the other groups. This is consistent with the conclusions drawn from mouse tumor weights and volumes. Figure 5f shows the HE staining images of the primary organ tissues of the mice. The hearts, livers, spleens, lungs, and kidneys did not show pathological damage after enhanced photodynamic therapy compared to the PBS group. As shown in Figure 6, the faster the Kaplan-Meier curve declined, the lower was the survival rate of the corresponding group. The median survival time of the BP@Au@FA-PEG + NIR group was 68 days, which was significantly longer than those of the other groups. These in vivo experiments demonstrated that the BP@Au@FA-PEG + NIR therapeutic system was biocompatible and could effectively treat HCC.

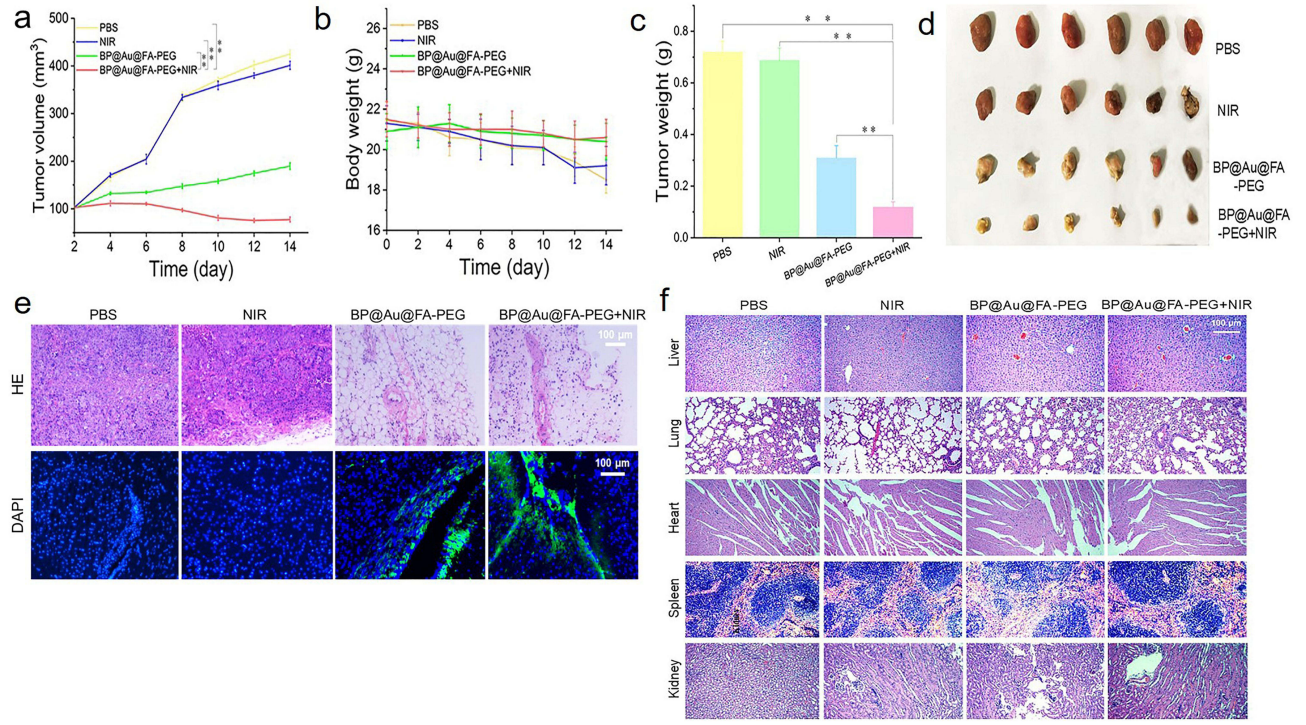

Figure 5 In vivo antitumor assays. Tumor volumes (**a**) and body weights (**b**) during treatment in mice. Histogram of tumor weights (**c**) and image of tumor tissue in mice after mortality (**d**). HE-stained images of tumor tissues (**e**) and major organs (**f**) in each experimental group. ** indicates a highly significant difference ($p< 0.01$).

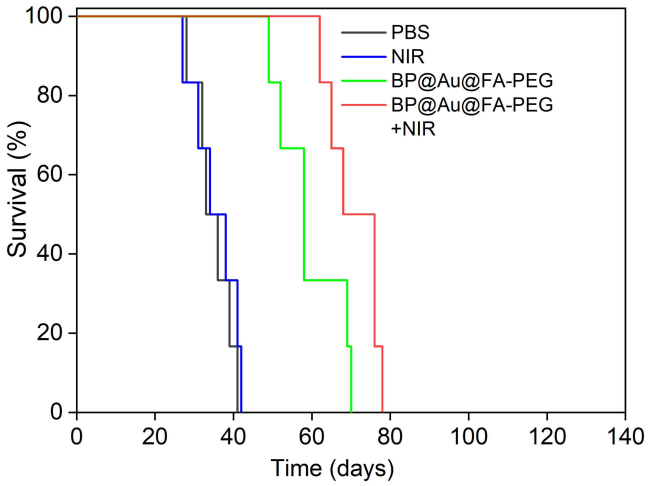

Figure 6 Survival analysis using Kaplan–Meier curves.

Conclusion

We successfully developed a BP@Au@FA-PEG nanoplatform for the targeted photodynamic therapy of HCC. Through a systematic process, the BP nanosheets were loaded with single-atom AuNPs. The introduction of FA with PEG chains not only bolstered the stability of BP nanosheets but also facilitated the specific targeting of HCC cells by exploiting the overexpression of folate receptors. In vitro experiments have shown that single-atom gold nanoenzymes effectively decompose H_2O_2 and generate a substantial quantity of •OH in tumor cells. Meanwhile, under 660 nm NIR, BP produced massive $^1O_2$. Both Au and BP can convert light to heat, thereby enhancing the efficacy of PDT. In vivo, experiments confirmed that BP@Au@FA-PEG significantly inhibited tumor growth without noticeable toxic side effects. These findings demonstrated the potential of BP@Au@FA-PEG as a promising therapeutic agent for cancer treatment.

Acknowledgments

This research was supported by Medicine and Health Research Foundation of Zhejiang Province (2024KY636) and Chun'an Special Eco-Functional Region Scientific Research Project (2024-11).

Disclosure

The authors declare no competing interests.

References

1. Su TS, Liang SX, Li LQ, et al. New staging model for radiation-based hepatocellular carcinoma treatment: a national multicenter study. *J Clin Transl Hepatol*. 2023;11(2):341–349. doi:10.14218/JCTH.2022.00002
2. Hao Y, Chen Y, He X, et al. RGD peptide modified platinum nanozyme co-loaded glutathione-responsive prodrug nanoparticles for enhanced chemo-photodynamic bladder cancer therapy. *Biomaterials*. 2023;293:121975. doi:10.1016/j.biomaterials.2022.121975
3. Du W, Chen W, Wang J, et al. A dual-nanozyme-loaded black phosphorus multifunctional therapeutic platform for combined photothermal/photodynamic/starvation cancer therapy. *J Mater Chem B*. 2023;11(23):5185–5194. doi:10.1039/d3tb00372h
4. Jin W, Chen Z, Wang Y, et al. Nano metal-photosensitizer based on Aza-BODIPY-Cu complex for CDT-enhanced dual phototherapy. *Chin Chem Lett*. 2024;35(7):109328. doi:10.1016/j.cclet.2023.109328
5. Gul EY, Karatas EA, Dogan HA, Karatas OF, Cosut B, Ecik ET. Erlotinib-modified BODIPY photosensitizers for targeted photodynamic therapy. *ChemMedChem*. 2023;18(2):e202200439. doi:10.1002/cmdc.202200439
6. Tao W, Zhu X, Yu X, et al. Black phosphorus nanosheets as a robust delivery platform for cancer theranostics. *Adv Mater*. 2017;29(1). doi:10.1002/adma.201603276
7. Zhou W, Pan T, Cui H, Zhao Z, Chu PK, Yu XF. Black phosphorus: bioactive nanomaterials with inherent and selective chemotherapeutic effects. *Angew Chem Int Ed Engl*. 2019;58(3):769–774. doi:10.1002/anie.201810878
8. Ma X, Zhu X, Huang C, Li Z, Fan J. Molecular mechanisms underlying the role of the puckered surface in the biocompatibility of black phosphorus. *Nanoscale*. 2021;13(6):3790–3799. doi:10.1039/d0nr08480h
9. Xu D, Liu J, Wang Y, Jian Y, Wu W, Lv R. Black phosphorus nanosheet with high thermal conversion efficiency for photodynamic/photothermal/immunotherapy. *ACS Biomater Sci Eng*. 2020;6(9):4940–4948. doi:10.1021/acsbiomaterials.0c00984

10. Li Z, Guo T, Hu Y, et al. A highly effective pi-pi stacking strategy to modify black phosphorus with aromatic molecules for cancer theranostics. *ACS Appl Mater Interfaces*. 2019;11(10):9860–9871. doi:10.1021/acsami.9b00374
11. Qiao K, Luo C, Huang R, et al. Ultrasound triggered tumor metabolism suppressor induces tumor starvation for enhanced sonodynamic immunotherapy of breast cancer. *Int J Nanomed*. 2023;18:3801–3811. doi:10.2147/IJN.S413543
12. Chen W, Du W, Zhang H, et al. Hemin-loaded black phosphorus-based nanosystem for enhanced photodynamic therapy and a synergistic photothermally/photodynamically activated inflammatory immune response. *Biomater Adv*. 2022;140:213091. doi:10.1016/j.bioadv.2022.213091
13. Cheng L, Wang X, Gong F, Liu T, Liu Z. 2D nanomaterials for cancer theranostic applications. *Adv Mater*. 2020;32(13):e1902333. doi:10.1002/adma.201902333
14. Ouyang J, Deng Y, Chen W, et al. Marriage of artificial catalase and black phosphorus nanosheets for reinforced photodynamic antitumor therapy. *J Mater Chem B*. 2018;6(14):2057–2064. doi:10.1039/c8tb00371h
15. Navyatha B, Singh S, Nara S. AuPeroxidase nanozymes: promises and applications in biosensing. *Biosens Bioelectron*. 2021;175:112882. doi:10.1016/j.bios.2020.112882
16. Liu CP, Wu TH, Liu CY, et al. Self-supplying O(2) through the catalase-like activity of gold nanoclusters for photodynamic therapy against hypoxic cancer cells. *Small*. 2017;13(26). doi:10.1002/smll.201700278
17. Wani IA, Jain SK, Khan H, Kalam A, Ahmad T. Gold nanoparticles as efficient catalysts in organic transformations. *Curr Pharm Biotechnol*. 2021;22(6):724–732. doi:10.2174/1389201022666210218195205
18. Lou-Franco J, Das B, Elliott C, Cao C. Gold nanozymes: from concept to biomedical applications. *Nanomicro Lett*. 2020;13(1):10. doi:10.1007/s40820-020-00532-z
19. Zhang X, Li G, Chen G, Wu D, Zhou X, Wu Y. Single-atom nanozymes: a rising star for biosensing and biomedicine. *Coord Chem Rev*. 2020;418. doi:10.1016/j.ccr.2020.213376
20. Qi P, Luo C, Pan Y, et al. Self-cascade catalytic single-atom nanozyme for enhanced breast cancer low-dose radiotherapy. *Colloids Surf B Biointerfaces*. 2023;227:113347. doi:10.1016/j.colsurfb.2023.113347
21. Li J, Hu B, Chen Z, et al. Mn(iii)-mediated carbon-centered radicals generate an enhanced immunotherapeutic effect. *Chem Sci*. 2024;15(2):765–777. doi:10.1039/d3sc03635a
22. Luo X, Zhang B, Zhang Y, et al. Rose bengal-modified gold nanorods for PTT/PDT antibacterial synergistic therapy. *Photodiagnosis Photodyn Ther*. 2022;39:102988. doi:10.1016/j.pdpdt.2022.102988
23. Wang Y, Chen Z, Li J, et al. A paramagnetic metal-organic framework enhances mild magnetic hyperthermia therapy by downregulating heat shock proteins and promoting ferroptosis via aggravation of two-way regulated redox dyshomeostasis. *Adv Sci*. 2024;11(11):e2306178. doi:10.1002/advs.202306178
24. Hu L, Liao H, Feng L, Wang M, Fu W. Accelerating the peroxidase-like activity of gold nanoclusters at neutral pH for colorimetric detection of heparin and heparinase activity. *Anal Chem*. 2018;90(10):6247–6252. doi:10.1021/acs.analchem.8b00885
25. Luo L, Luo J, Li H, et al. Water enables mild oxidation of methane to methanol on gold single-atom catalysts. *Nat Commun*. 2021;12(1):1218. doi:10.1038/s41467-021-21482-z